IOPscience iopscience.iop.org

Home Search Collections Journals About Contact us My IOPscience

Fe-Tb alloy films prepared by ion beam-assisted deposition

This article has been downloaded from IOPscience. Please scroll down to see the full text article.

2002 J. Phys.: Condens. Matter 14 1775

(http://iopscience.iop.org/0953-8984/14/8/307)

View the table of contents for this issue, or go to the journal homepage for more

Download details:
IP Address: 171.66.16.27
The article was downloaded on 17/05/2010 at 06:12

Please note that terms and conditions apply.

INSTITUTE OF PHYSICS PUBLISHING JOURNAL OF PHYSICS: CONDENSED MATTER

J. Phys.: Condens. Matter **14** (2002) 1775–1784 PII: S0953-8984(02)28585-9

Fe–Tb alloy films prepared by ion beam-assisted deposition

F Yang, T He, F Zeng and F Pan

Laboratory of Advanced Materials, Department of Materials Science and Engineering, Tsinghua University, Beijing 100084, People's Republic of China

Received 6 September 2001, in final form 27 October 2001
Published 15 February 2002
Online at stacks.iop.org/JPhysCM/14/1775

Abstract

Fe–Tb multilayers and alloy films prepared by sputtering or evaporation are found to have perpendicular magnetic anisotropy. In this work, Fe–Tb alloy films with parallel magnetic anisotropy in a wide composition range, 3–30 at.% Tb, are obtained for the first time, prepared by the ion beam-assisted deposition technique. All the films have an easy magnetization axis in the film plane. A supersaturated bcc solid solution phase with enlarged lattice and increased saturation magnetization is obtained in the range of 6.5–13 at.% Tb; while in the range of 21–30 at.% Tb, the films are amorphous and have lower saturation magnetization. Thermodynamic calculation of the Gibbs free energy of the Fe–Tb system shows that both the bcc solid solution and the amorphous phase are energetically and dynamically favoured in the two composition regions, respectively.

1. Introduction

Many rare earth–transition metal (RETM) compounds, crystalline or amorphous, have a commercial potentiality ranging from permanent magnets to information storage media. Among them, ferromagnetic films consisting of rare earth and transition metals are interesting systems, because the phenomenon of perpendicular magnetic anisotropy (PMA) can be used in high-density recording (e.g. [1]) and a sufficiently large Kerr effect can serve as magneto-optic (MO) recording media [2]. For these reasons, much attention has been paid to the RE–Fe system, especially Tb–Fe films. Studies of Fe/Tb multilayers show that the magnetic ordering in the interface is the main origin of PMA [3, 4]. Amorphous Fe–Tb alloy films also exhibit strong PMA due to preferred structure orientation [5, 6]. In a word, structure anisotropy in the perpendicular direction induces PMA, even in alloy films without artificial structure anisotropy. Based on this theory, it can be deduced that Fe–Tb films without structural orientation anisotropy may have no PMA, yet such films have been observed in a very limited composition range, i.e. when Tb content is less than 5 at.% [7, 8].

0953-8984/02/081775+10$30.00 © 2002 IOP Publishing Ltd Printed in the UK

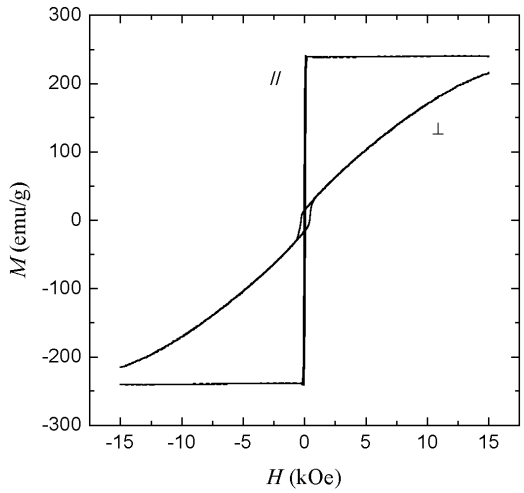

Figure 1. Hysteresis loops in directions perpendicular and parallel to film plane measured for $Fe_{92}Tb_8$ film.

Since ion beam mixing is a useful technique to obtain homogeneous films both in chemical composition and structure, Fe–Tb alloy films are fabricated by ion beam-assisted vapour deposition to investigate the magnetic performance of an evenly structured Fe–Tb film. Films without PMA are obtained in the range of 3–30 at.% Tb. From another point of view, the results confirm that structure anisotropy is the origin of PMA in RETM films.

2. Experimental details

Fe–Tb films are prepared by an ion beam-assisted deposition (IBAD) apparatus consisting of an ion beam source and an electron beam evaporator, a sketch of which is shown in figure 1 of [9]. Fe and Tb are alternately electron beam deposited onto freshly cleaved NaCl single crystals and glass substrates, while at the same time bombarded with an Ar^+ ion beam provided by an 8 cm-diameter Kaufmann ion source. The background vacuum before deposition is 8×10^{-5} Pa and the samples are deposited at a working argon pressure of 4.5×10^{-3} Pa. To make a uniform mixing of the two metals, the incident ion beam is set normal to the substrate surface. Ion bombardment energy is kept at 3 keV and the ion beam current density is fixed at 12 μA cm^{-2}. Deposition rates for Fe and Tb are both 0.03 nm s^{-1}. Film thickness is monitored by an *in situ* quartz crystal oscillator and kept at 50–60 nm. By changing the individual Fe and Tb layer thickness, the overall composition of the Fe–Tb films are adjusted to be in the range of 3–30 at.% Tb. The modulation wavelengths of Fe/Tb bilayers for alternate e-beam deposition are around 5 nm, which is smaller than the ion project range calculated by SRIM [10], so a homogeneous blending is achieved in the films. Transmission electron microscope (TEM) bright field (BF) observation and selected area diffraction (SAD) are made for microstructure analyses. M–H hysteresis loops are measured in fields up to 15 kOe with an alternate gradient magnetometer (AGM). The films are dissolved in HCl after magnetic measurements and inductively coupled plasma spectroscopy (ICP) is used to determine the Fe and Tb contents in the samples.

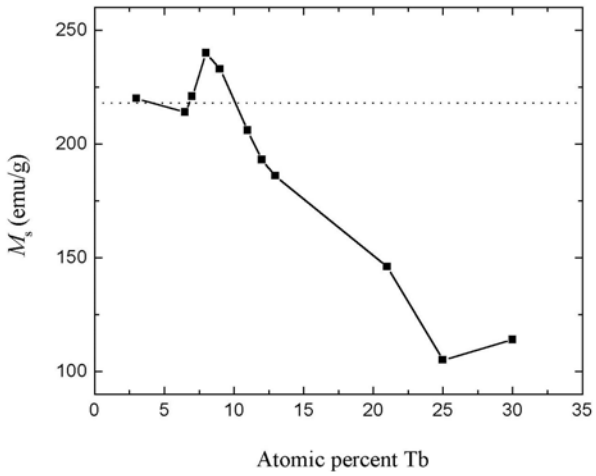

Figure 2. Saturated magnetization of IBAD Fe–Tb films versus Tb content.

3. Results and discussion

3.1. Phases formed by IBAD and their properties

With Tb content less than 30 at.%, the measured hysteresis loops of all the IBAD Fe–Tb films at ambient temperature have an easy magnetization axis in the film plane and small coercivity (a few dozens of Oe) in that direction, the M–H loops of one typical sample are shown in figure 1. Saturation magnetization M_s values are deduced from the easy axis curves and are presented corresponding to measured chemical composition in figure 2. The error for M_s value in our experiment is estimated to be less than 4%. As Tb content increases and Fe content decreases, M_s of the alloy films decrease, except for a peak between 6.5 and 12 at.% Tb and a valley at 25 at.% Tb. By considering different M_s values together with unlike structures and morphologies, the overall range is separated into three regions: 3 at.% Tb, 6.5–13 at.% Tb, and 21–30 at.% Tb. The properties of IBAD Fe–Tb films are discussed in the three regions.

3.1.1. 3 at.% Tb: region close to bcc Fe. The composition of this region is quite close to that of pure iron. There is only one set of clear Fe diffraction rings discernable in the SAD pattern of the $Fe_{97}Tb_3$ film, as shown in figure 3(*a*). As figure 2 shows, the measured M_s of that sample is 220 emu g^{-1}, which is very close to that of bulk iron, 218 emu g^{-1} [11].

The BF image of the sample has an interesting feature of numerous tiny needle-like crystals, as shown in figure 4(*a*). It is traced to the ion irradiation, which has a similar kinetic effect as rapid quenching, and calculations show that needle crystal growth is likely to occur in undercooling circumstances [12, 13].

3.1.2. 6.5–13 at.% Tb: supersaturated bcc solid solution. In this region, SAD patterns of the films have only one set of bcc crystalline diffraction rings, which imply a supersaturated solid solution, as figure 3(*b*) shows. The equilibrium solubility of Tb in bcc Fe is less than 1 at.% at ambient temperature [14]. In addition, the intermetallic compounds like $Fe_{17}Tb_2$ (hexagonal or rhombohedral), $Fe_{23}Tb_6$ (cubic), Fe_3Tb (rhombohedral), and Fe_2Tb (rhombohedral) do not have a bcc structure. It can be concluded that a Fe-based bcc supersaturated solid solution is obtained in the range of 6.5–13 at.% Tb. Calibrated SAD quantitative analyses show that the

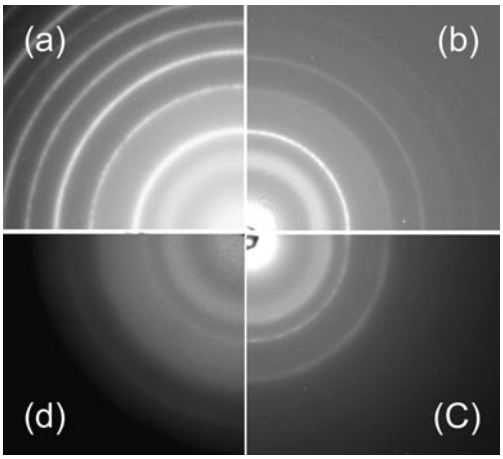

Figure 3. SAD patterns of IBAD Fe–Tb films: (*a*) $Fe_{97}Tb_3$, (*b*) $Fe_{92}Tb_8$, (*c*) $Fe_{79}Tb_{21,}$ and (*d*) $Fe_{70}Tb_{30}$.

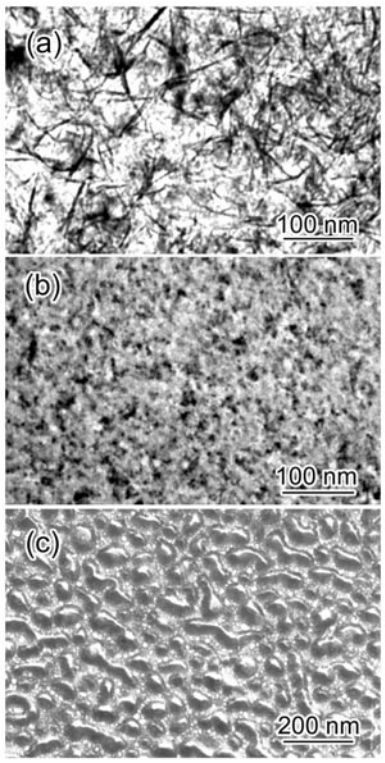

Figure 4. Typical morphology of IBAD Fe–Tb films under TEM BF observation: (*a*) $Fe_{97}Tb_3$, (*b*) $Fe_{92}Tb_8$ and (*c*) $Fe_{75}Tb_{25}$.

bcc lattice constant expands in the solid solution compared to that of bulk iron. For example, the cubic cell length of $Fe_{92}Tb_8$ is measured to be 2.908 ± 0.005 Å and that of bulk Fe is 2.866 Å. Since Tb atoms are much bigger than Fe atoms, the substitutional solid solution should have a dilated lattice.

Corresponding to that range there is a peak in the M_s-composition chart of figure 2. The top of the peak is at $Fe_{92}Tb_8$, where the saturation magnetization is up to 240 emu g^{-1}, which is larger than M_s of bulk Fe, 218 emu g^{-1}. The bcc solid solution is ferromagnetic, as shown in figure 1. Ion irradiation during the film growth removes macroscopic structure anisotropy as well as macroscopic magnetic coupling between Fe–Tb pairs. The expanded lattice may be the reason for increased M_s according to calculations [15].

In TEM BF observation, the films in this range show evenly distributed tiny crystals, as illustrated in figure 4(*b*). The grain size of these crystals is estimated to be no more than 20 nm.

To study the stability of the bcc solid solution, the structure of IBAD Fe–Tb films is re-examined after keeping at room temperature in dry air for 60 days. Although the films have lost their original metallic lustre and change colour from argent to light yellow, even TEM observation shows some oxidation; SAD of the films reveal that the bcc solid solution still exists in some unoxidized areas of the film. The results evince that the solid solution does not decompose into separated Fe and Tb phases upon ageing at room temperature for 60 days.

3.1.3. 21–30 at.% Tb: partially amorphous phase. Films in this region have a much lower M_s value, i.e. smaller than 150 emu g^{-1}. In figures 3(*c*) and (*d*), the SAD patterns show a partially amorphous structure different from the former bcc structure. $Fe_{79}Tb_{21}$ has diffused loops and only Fe(110) but no other diffraction rings are discernable, as shown in figure 3(*c*); $Fe_{70}Tb_{30}$ has only halos and no rings at all, as shown in figure 3(*d*). The results indicate that the transition from crystalline to amorphous in IBAD Fe–Tb films does not occur abruptly but gradually with the increasing of Tb content. In fact the amorphization of the iron phase is the reason for the decreasing of magnetization. It should also be noted that the lowest M_s is observed at $Fe_{75}Tb_{25}$, which has a composition close to 23 at.% Tb, the magnetic compensation composition of the Fe–Tb system [8, 16].

Quite different to crystalline structure, the amorphous films in this region have a fractal-like pattern morphology. Similar morphology has been observed in other ion-irradiated films [17, 18].

3.2. Parallel magnetic anisotropy of IBAD Fe–Tb films

In previous studies, Tb content of films with in-plane easy axis is found to be no more than 10 at.% in rf-sputtered films [7]. Investigation in sputtering or vapour-deposited Tb/Fe multilayers all show PMA due to the coupling effect when the Fe layer is thinner than 2.0 nm [19, 20]. In addition, co-sputtering or co-evaporation deposited Fe–Tb amorphous films have PMA in the range of 15–30 at.% Tb [7, 16, 21, 22]. The reason for the anisotropy has been studied by various methods. By using linear polarized synchrotron radiation x-ray absorption, Fujiwara *et al* [3,23] have proposed a structural anisotropy of the Fe–Tb interface in multilayers as the origin of PMA; while in vapour-deposited amorphous Tb–Fe alloy films, the preferred orientation of local adatom configuration could lead into energetically favourable orientation by minimizing surface energy during deposition, i.e. these amorphous films are structurally anisotropic, so the films exhibit PMA [5, 24].

In contrast, the Fe–Tb films prepared by IBAD all have in-plane magnetization when Tb content is less than 30 at.%. Ion irradiation has three effects in Fe–Tb multilayers: the demixing of Fe and Tb atoms at the interface, the mixing of layers, and the creation of defects in the core of the bcc ion layers. With increasing ion fluence, the mixing effects increase significantly yet the demixing effects decrease [25]. It is also found in Fe/Tb multilayers that ion irradiation produces a rougher interface and decreasing PMA [26]. Since ion beams are

bombarding continuously during film growth, the reorientation and consequent freezing [27] in thermally evaporated Fe–Tb alloy film are totally disrupted by the atomic collision cascade triggered by impinging ions [28]. Thus the short-range order of an Fe–Tb pair is non-existent due to the mixing effect of ion bombardment, the film having parallel magnetic anisotropy as other Fe–ME film, i.e. the macroscopic shape anisotropy energy of the film makes the in-plane direction the easy axis of magnetization. On the other hand, it can be concluded that the short-range order of an Fe–Tb pair is the main origin of PMA in Fe–Tb multilayers.

The SAD patterns of the Fe–Tb films have a relatively strong Fe(110) diffraction ring in the range of 6.5–28 at.% Tb. It has been found that films tend to have texture in the film plane during IBAD [29] and the electrical and magnetic properties are strongly affected by the texture. The resulting shape anisotropy is found to be responsible for in-plane anisotropy in cobalt and nickel magnetic films [30]. Thus, the bcc (110) texture may be another factor that contributes to the in-plane anisotropy of Fe–Tb films.

3.3. Thermodynamic calculation of Fe–Tb system

3.3.1. Thermodynamic model and construction of free-energy diagram. In IBAD Fe–Tb films the formation of the bcc solid solution and amorphous phase, which are both metastable phases, is a process far from equilibrium as a whole; consequently, some kinetic factors would play an important role in influencing the phase formation. The ion mixing process is generally divided into three steps [28]: first the atomic collision cascade triggered by impinging ions, second the relaxation and third the delayed period. Whether crystalline or amorphous, the structure of an alloy phase is fixed during the second step, as numerous atoms are excited to be in motion during the first step. In the first step, as the energy of the irradiation ions is on the order of several hundred keV, which is much higher than the typical binding energy of the solids (5–10 eV), the irradiating ions would trigger a series of atomic collisions, which is called the atomic collision cascade. This step is definitely far from equilibrium. After receiving an adequate ion dose, the layered structure of the originally multilayered film is totally blended into a homogeneous mixture of Fe and Tb, which is a highly energetic state. At the moment of the termination of the first step, the high-energy state would relax towards lower energy states and the system begins the second step, relaxation. It is at this very moment that the equilibrium thermodynamics comes into play and governs the direction of the relaxation. The possible lower energy state is thus decided and later conserved to form the metastable phase that is observed in experiments. In this sense, the free-energy calculation based on equilibrium thermodynamics can be applied to discuss metastable phase formation during the relaxation period [31, 32].

In this work, Miedema *et al* 's [33] and Liu and Zhang's [32] models are applied to calculate the free-energy curves of bcc and amorphous phases, and then a Gibbs free-energy diagram of the system is constructed for discussing the thermodynamic possibility of metastable phase formation in the Fe–Tb system. As a semi-empirical one, the model has successfully interpreted the phase evolution in various bi-metal systems upon ion irradiation [34–39], and we will show that it obtains a satisfactory result for the Fe–Tb system.

The free energy of mixing is given by $\Delta G = \Delta H - T\Delta S$, where ΔH and ΔS are the enthalpy and entropy of mixing, respectively. Taking the expression for the entropy of mixing, as a first approximation, as that of an ideal solid solution [40], we obtain

$$\Delta S = -R(X_A \ln X_A + X_B \ln X_B) \tag{1}$$

where R is the gas constant, X_A and X_B are the atomic concentration of A and B atoms, respectively. According to Lopez *et al* [41,42], the enthalpy of the formation of a substitutional solid solution of transition metals can be expressed as the sum of three terms:

$$\Delta H_s = \Delta H_s^c + \Delta H_s^e + \Delta H_s^s \tag{2}$$

where ΔH_s^c, ΔH_s^e, ΔH_s^s represent the chemical contribution, elastic contribution and structure contribution, respectively.

In this equation, ΔH_s^c is the chemical contribution due to the electron redistribution that occurs when the alloy is formed, and it is given by [43] as

$$\Delta H_s^c = \Delta H_{amp} X_A V_A^{2/3} f_A^B \tag{3}$$

in which V_A is the atomic volume of atom A, f_A^B is a function that accounts for the total area of contact between A and B atomic cells [42], and ΔH_{amp} is an amplitude concerning the magnitude of the electron redistribution interaction and is a constant for a specific system, e.g. -17.621 kJ mol $^{-1}$cm^{-2} for the Fe–Tb system.

ΔH_s^e in equation (2) is the elastic contribution from atomic size mismatch to the enthalpy of the solid solution mixing. This term justifies the well-known Hume–Rothery rules stating that a substantial atomic size mismatch prevents the formation of a substitutional solid solution. This contribution can be derived from the equation

$$\Delta H_s^e = X_A X_B [X_B \Delta H_e(A \text{ in } B) + X_A \Delta H_e(B \text{ in } A)] \tag{4}$$

where ΔH_e (i in j) is the elastic contribution to the heat of solution of i in j, a detailed interpretation can be referred to in [33].

The third term in equation (2), ΔH_s^s, reflects the correlation between the number of valence electrons and the crystalline structure of transition metals [44], as

$$\Delta H_s^s = E(Z_m) - X_A E_A(Z_A) - X_B E_B(Z_B) \tag{5}$$

where Z_m is the average number of valence (s + d) electrons per atom in the alloy, and E, E_A, and E_B are the lattice stabilities of the alloy and two pure components, respectively. In our calculation, the parameters are referred to in [45,46]

On the other hand, the enthalpy of the amorphous alloy phase [45] can be written as

$$\Delta H_{amor} = \Delta H_{amor}^c + \alpha(X_A T_{m,A} + X_B T_{m,B}) \tag{6}$$

where α is an empirical parameter being 3.5 J mol^{-1} K^{-1}, and $T_{m,i}$ is the melting point of component i. ΔH_{amor}^c is the chemical contribution of the amorphous phase, and can be calculated the same way as equation (3) for a substitutional solid solution. The second term of equation (6) is an extra enthalpy caused by the difference of the reference states between amorphous and solid solution phases.

By using the model mentioned earlier, the free-energy change of the formation of the solid solution and amorphous phase is calculated for the Fe–Tb binary system.

3.3.2. Interpretation of the experimental results based on the calculated free-energy diagram. Setting the equilibrium mixture of the two constituent metals as the reference state, figure 5 shows the calculated Gibbs free-energy curves of the Fe-rich bcc solid solution crystalline phase and amorphous phase in the range of 0–30 at.% Tb, and the results can interpret the experimental results in a satisfactory way. Firstly, the Gibbs free energy (ΔG) of the bcc solid solution, as the left part of the chart shows, remains negative for Tb content lower than 16 at.% Tb, which implies that the bcc state is actually the most stable in that composition range. In fact, we obtain the bcc solid solution in the range below 13 at.% Tb. Also in this region, the amorphous state has a positive ΔG, showing a more unstable state than the

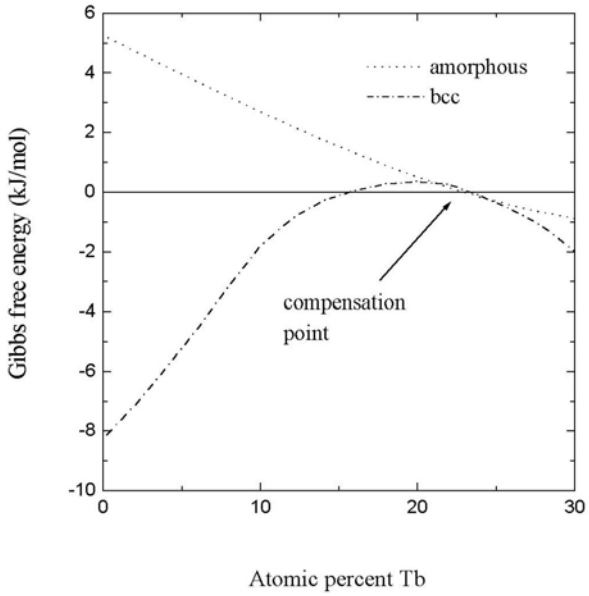

Figure 5. Calculated Gibbs free-energy diagram of the Fe–Tb system as a function of atomic composition.

mechanical mixture of Fe and Tb. Secondly, ΔG_{bcc} increases to positive and obtains its peak value at 20 at.% Tb, where the $\Delta G_{amorphous}$ reduces to a value close to that of ΔG_{bcc}. Thirdly, further decreasing of $\Delta G_{amorphous}$ obtains negative values when Tb content exceeds 23%, which is the exact point of magnetic compensation. Considering dynamic factors, it is clear that there is a large energy gap between the reference state and the bcc solid solution, which offers a great driving force for the formation of the bcc phase.

For Tb content over 23 at.%, although the bcc phase has a lower-E state than the amorphous phase, the difference is quite small, i.e. smaller than 1.0 kJ mol^{-1}, so the driving force of phase transformation is possibly smaller than the energy barrier. Normally the span of the collision cascade and relaxation process induced by impacting Ar^+ is very short, lasting for only 10^{-10}–10^{-9} s; the temperature rise in the materials goes up to 10^3–10^4 K in such a transient time, so the phases formed during ion bombardment only take simple forms such as bcc, fcc, or amorphous [32]. The amorphous structure is even simpler than the bcc structure when the system transforms from the ion-blended mixture to the alloy phase, which means that the energy barrier is comparatively large. In addition, the mixing ion has an energy of 3 keV, which has a significant blending effect [25]. On the other hand, the heat of mixing for Fe–Tb is about -4 kJ/mole of atoms when Fe has the same atoms of Tb [33]. Furthermore, the atomic radiuses of Fe and Tb atoms are 1.241 and 1.782 Å, respectively, i.e. the difference between the two radiuses is as large as 43.6%. These two kinetic facts favour a solid-state amorphization reaction (SSAR) [47] between Fe and Tb. In fact, the experiments show that Fe–Tb films are indeed partially amorphous when Tb content exceeds 21 at.%.

As a summary, by the Gibbs free-energy calculation and considering dynamic factors, it is concluded that the bcc solid solution forms when Tb content is below 13 at.% since it is an energetic favourable state with lowest Gibbs free energy; the partially amorphous phase is formed when Tb content surpasses 21 at.% because it is both a low energy state and a kinetically preferred state.

4. Conclusion

Fe–Tb alloy films are fabricated by IBAD in the composition range of 3–30 at.% Tb. A new phase, the bcc solid solution, is obtained in the range of 6.5–13 at.% Tb. The bcc solid solution has an expanded lattice and higher saturated magnetization compared to that of bulk iron. When Tb content exceeds 21%, the IBAD Fe–Tb films are amorphous with low magnetizations. All the films exhibit an easy magnetization axis in the film plane, which is induced by a full mixing of atoms with ion beam irradiation and consequent homogeneous structure. The result strongly confirms that PMA in other sputtered or evaporation deposited Fe–Tb films are related to the short-range order of Fe–Tb pairs. Furthermore, thermodynamic calculation of the Gibbs free-energy of the Fe–Tb system shows that both the bcc solid solution and the amorphous phase are energetically favoured and the composition ranges of the calculated results resemble those obtained by experiment.

Acknowledgments

We are indebted to Professor Liu B X for his helpful discussions and Dr Li Z F for dynamic calculations. Financial aid from the National Natural Science Foundation of China (grant no 59971025), the Ministry of Science and Technology of China (grant no G2000067207-1), and the Administration of Tsinghua University is gratefully acknowledged.

References

[1] Wang Y J and Kleemann W 1991 *Phys. Rev.* B **44** 5132
[2] Guarisco D, Burgermeister R, Stamm C and Meier F 1996 *Appl. Phys. Lett.* **68** 1729
[3] Fujiwara Y, Yu X Y, Tsunashima S and Iwata S 1996 *J. Appl. Phys.* **79** 6270
[4] Freitag A E and Chowdhury A R 1996 *J. Appl. Phys.* **85** 4696
[5] Hellman F and Gyorgy E M 1992 *Phys. Rev. Lett.* **68** 1391
[6] Harris V G, Aylesworth K D, Elam W T and Koon N C 1992 *J. Alloys Compounds* **191** 431
[7] Mimura Y and Imamura N 1976 *Appl. Phys. Lett.* **28** 746
[8] Hellman F, van Dover R B, Nakahara S and Gyorgy E M 1989 *J. Magn. Magn. Mater.* **81** 234
[9] Ding M, Zeng F and Pan F 2000 *Nucl. Instrum. Methods Phys. Res.* B **170** 79
[10] Ziegler J F and Biersack J P 2000 Computer code SRIM2000
[11] Cullity B D 1972 *Introduction to Magnetic Materials* (Reading, MA: Addison-Wesley) p 617
[12] Brener E A and Temkin D E 1989 *Europhys. Lett.* **10** 171
[13] Provatas N, Goldenfeld N, Dantzig J, LaCombe J C, Lupulescu A, Koss M B, Glicksman M E and Almgren R 1999 *Phys. Rev. Lett.* **82** 4496
[14] Massalski T B 1990 *Binary Alloy Phase Diagrams* 2nd edn (Materials Park, OH: ASM International) p 1779
[15] Moruzzi V L, Marcus P M and Kübler J 1989 *Phys. Rev.* B **39** 6957
[16] Kim M J, Bow J S, Carpenter R W, Liu J, Kim S G, Lee S K, Kim W M and Yoon J S 1994 *IEEE Trans. Magn.* **30** 4398
[17] Choi C-H and Barnett S A 1994 *J. Cryst. Growth* **137** 381
[18] Zhu H N, Gao K Y and Liu B X 2000 *Phys. Rev.* B **62** 1647
[19] Shan Z S and Sellmyer D J 1990 *Phys. Rev.* B **42** 10 433
[20] Lanchava B and Hoffmann H 1999 *J. Magn. Magn. Mater.* **192** 403
[21] Hellman F, van Dover R B, Nakahara S and Gyorgy E M 1989 *J. Magn. Magn. Mater.* **81** 234
[22] Van Dover R B, Hong M, Gyorgy E M, Dillon J F Jr and Albiston S D 1985 *J. Appl. Phys.* **57** 3897
[23] Fujiwara Y, Masaki T, Yu X Y, Sakurai M, Tsunashima S, Iwata S and Suzuki K 1997 *J. Appl. Phys.* **36** 5097
[24] Hellman F 1994 *Appl. Phys. Lett.* **64** 1947
[25] Teillet J, Richomme F, Fnidiki A and Toulemonde M 1997 *Phys. Rev.* B **55** 11 560
[26] Gupta A, Paul A, Gupta R, Avasthi D K and Principi G 1998 *J. Phys.: Condens. Matter* **10** 9669
[27] Hellman F, Messer M and Abarra E N 1999 *J. Appl. Phys.* **86** 1047
[28] Zhang Z J and Liu B X 1994 *J. Appl. Phys.* **73** 3315
[29] Ensinger W 1998 *Surf. Coat. Technol.* **99** 1

[30] Šikola T *et al* 1999 *Nucl. Instrum. Methods Phys. Res.* B **148** 907
[31] Yang G W, Lin C and Liu B X 1999 *J. Mater. Res.* **14** 3027
[32] Liu B X, Lai W S and Zhang Q 2000 *Mater. Sci. Eng.* **R29** 1
[33] Miedema A R, Niessen A K, de Boer F R, Boom R and Mattens W C M 1989 *Cohesion in Metals: Transition Metal Alloys* (Amsterdam: North-Holland)
[34] Liu B X and Zhang Z J 1994 *Phys. Rev.* B **49** 12 519
[35] Brewer W D, Hauf S, Jones D, Frotapessoa S, Kapoor J, Li Y, Metz A and Riegel D 1995 *Phys. Rev.* B **51** 12 595
[36] Sato H, Kitakami O, Sakurai T, Shimada Y, Otani Y and Fukamichi K 1997 *J. Appl. Phys.* **81** 1858
[37] Pacaud J, Jaouen C and Gladyszewski G 1999 *J. Appl. Phys.* **86** 4847
[38] Li Z F, Lai W S and Liu B X 2000 *Appl. Phys. Lett.* **77** 3920
[39] Li Z F, Zhang Q, Yu D P, Liu C and Liu B X 2001 *Phys. Rev.* B **64** 014102
[40] Zhang Z J, Bai H Y, Qiu Q L, Yang T, Tao K and Liu B X 1993 *J. Appl. Phys.* **73** 1702
[41] Lopez J M and Alonso J A 1985 *Z. Naturforsch. A* **40** 1199
[42] Weeber A W 1987 *J. Phys. F: Met. Phys.* **17** 809
[43] Niessen A K, de Boer F R, Boom R, de Chatel P F, Mattens W C M and Miedema A R 1983 *CALPHAD, Comput. Coupling Phase Diagr. Thermochem.* **7** 51
[44] Alonso J A, Gallego L J, Somoza J A and Liu B X 1991 *Thin Films and Beam-Solid Interactions* ed L Huang (Amsterdam: Elsevier) p 297
[45] Niessen A K and Miedema A R 1983 *Ber. Bunsenges. Phys. Chem.* **87** 717
[46] Niessen A K, Miedema A R, de Boer F R and Boom R 1988 *Physica* B **151** 401
[47] Schwarz R B and Johnson W L 1983 *Phys. Rev. Lett.* **51** 415